Generalized Michaelis–Menten rate law with time-varying molecular concentrations

Roktaek Lim[1,7], Thomas L. P. Martin[1,7], Junghun Chae[2,7], WooJoong Kim[2], Cheol-Min Ghim[2,3,*], and Pan-Jun Kim[1,4,5,6,*]

[1]Department of Biology, Hong Kong Baptist University, Kowloon, Hong Kong

[2]Department of Physics, Ulsan National Institute of Science and Technology, Ulsan 44919, Republic of Korea

[3]Department of Biomedical Engineering, Ulsan National Institute of Science and Technology, Ulsan 44919, Republic of Korea

[4]Center for Quantitative Systems Biology & Institute of Computational and Theoretical Studies, Hong Kong Baptist University, Kowloon, Hong Kong

[5]State Key Laboratory of Environmental and Biological Analysis, Hong Kong Baptist University, Kowloon, Hong Kong

[6]Abdus Salam International Centre for Theoretical Physics, 34151 Trieste, Italy

[7]R.L., T.L.P.M., and J.C. contributed equally to this work.

[*]For correspondence:
C.-M.G. (email: cmghim@unist.ac.kr) or P.-J.K. (email: panjunkim@hkbu.edu.hk).

Abstract

The Michaelis–Menten (MM) rate law has been the dominant paradigm of modeling biochemical rate processes for over a century with applications in biochemistry, biophysics, cell biology, and chemical engineering. The MM rate law and its remedied form stand on the assumption that the concentration of the complex of interacting molecules, at each moment, approaches an equilibrium much faster than the molecular concentrations change. Yet, this assumption is not always justified. Here, we relax this quasi-steady state requirement and propose the generalized MM rate law for the interactions of molecules with active concentration changes over time. Our approach for time-varying molecular concentrations, termed the effective time-delay scheme (ETS), is based on rigorously estimated time-delay effects in molecular complex formation. With particularly marked improvements in protein–protein and protein–DNA interaction modeling, the ETS provides an analytical framework to interpret and predict rich transient or rhythmic dynamics (such as autogenously-regulated cellular adaptation and circadian protein turnover), which goes beyond the quasi-steady state assumption.

Introduction

Since proposed by Henri [1] and Michaelis and Menten [2], the Michaelis–Menten (MM) rate law has been the dominant framework for modeling the rates of enzyme-catalyzed reactions for over a century [1–4]. The MM rate law has also been widely adopted for describing other bimolecular interactions, such as reversible binding between proteins [5–7], between a gene and a transcription factor [8,9], and between a receptor and a ligand [10,11]. The MM rate law hence serves as a common mathematical tool in both basic and applied fields, including biochemistry, biophysics, pharmacology, and many subfields of chemical engineering [12]. The derivation of the MM rate law from the underlying biochemical mechanism is based on the steady-state approximation by Briggs and Haldane [3], referred to as the *standard quasi-steady state approximation* (sQSSA) [12–14]. The sQSSA, however, is only valid when the enzyme concentration is low enough and thus the concentration of enzyme–substrate complex is negligible compared to substrate concentration [14]. This condition may be acceptable for many metabolic reactions with substrate concentrations that are typically far higher than the enzyme concentrations.

Nevertheless, in the case of protein–protein interactions in various cellular activities, the interacting proteins as the “enzymes” and “substrates” often show the concentrations comparable with each other [15–17]. Therefore, the use of the MM rate law for describing protein–protein interactions has been challenged in its rationale, with the modified alternative formula from the *total quasi-steady state approximation* (tQSSA) [12,13,18–24]. The tQSSA-based form is generally more accurate than the MM rate law from the sQSSA, for a broad range of combined molecular concentrations and thus for protein–protein interactions as well [12,13,18–24]. The superiority of the tQSSA has not only been proven in the quantitative, but also in the qualitative outcomes of systems, which the sQSSA sometimes fails to predict [12,18]. Later, we will provide the overview of the tQSSA and its relationship with the conventional MM rate law from the sQSSA.

Despite the correction of the MM rate law by the tQSSA, both the tQSSA and sQSSA still rely on the assumption that the concentration of the complex of interacting molecules, at each moment, approaches an equilibrium much faster than the molecular concentrations change [12,14,21]. Although this quasi-steady state assumption may work for a range of biochemical systems, the exact extent of such systems to follow that assumption is not clear. Numerous cellular processes do exhibit active molecular concentration changes over time, such as in signal responses, circadian oscillations, and cell cycles [6,7,18,25–28], calling for a

better approach to even cover the time-varying molecular concentrations that may not strictly adhere to the quasi-steady state assumption.

In this study, we report the generalization of the MM rate law, whereby the interaction of time-varying molecular components is more properly described than by the tQSSA and sQSSA. This generalization is the correction of the tQSSA with rigorously estimated, time-delay effects affected by free molecule availability. Our formulation, termed the effective time-delay scheme (ETS), well accounts for the transient or oscillatory dynamics and empirical patterns of biomolecular systems with the relevant analytical insights, which are not captured by the previous methods. Surprisingly, we reveal that the existing quasi-steady state assumption can even fail for extremely slow changes in protein concentrations under autogenous regulation, whereas the ETS does not. In addition, the ETS allows the natural explanation of rhythmic degradation of circadian proteins without requiring explicitly-rhythmic post-translational mechanisms; this is not straightforward within the quasi-steady state assumption. As an added feat, the ETS improves kinetic parameter estimation. As demonstrated in a number of contexts such as autogenously-regulated cellular adaptation and circadian oscillations, our approach offers a unified theoretical framework to interpret and predict rich transient or rhythmic dynamics of biochemical systems with a wide range of applications.

Results

Theory overview

First, we present the outline of the tQSSA, sQSSA, and our generalized MM rate law. Consider two different molecules A and B that bind to each other and form complex AB, as illustrated in Fig. 1(A). For example, A and B may represent two participant proteins in heterodimer formation, a chemical substrate and an enzyme in a metabolic reaction, and a solute and a transporter in membrane transport. The concentration of the complex AB at time t, denoted by $C(t)$, changes over time as in the following equation:

$$\frac{\mathrm{d}C(t)}{\mathrm{d}t} = k_{\mathrm{a}}[A(t) - C(t)][B(t) - C(t)] - k_{\delta}C(t). \quad (1)$$

Here, $A(t)$ and $B(t)$ denote the total concentrations of A and B, respectively, and hence $A(t) - C(t)$ and $B(t) - C(t)$ correspond to the concentrations of free A and B. k_{a} denotes the association rate of free A and B. k_{δ} is the effective "decay" rate of AB with $k_{\delta} \equiv k_{\mathrm{d}} + r_{\mathrm{c}} + k_{\mathrm{loc}} + k_{\mathrm{dlt}}$ where k_{d}, k_{loc}, and k_{dlt} stand for the dissociation, translocation, and

dilution rates of AB, respectively, and r_c for the chemical conversion or translocation rate of A or B upon the formation of AB [Fig. 1(A)].

In the tQSSA, the assumption is that $C(t)$ approaches the equilibrium fast enough each time, given the values of $A(t)$ and $B(t)$ [12,21]. This assumption and the notation $K \equiv k_\delta/k_a$ lead Eq. (1) to an estimate $C(t) \approx C_{tQ}(t)$ with the following form (Supplementary Material, Section S1):

$$C_{tQ}(t) \equiv \frac{1}{2}\{K + A(t) + B(t) - K\Delta_{tQ}(t)\}, \tag{2}$$

$$\Delta_{tQ}(t) \equiv \sqrt{\left[1 + \frac{A(t)+B(t)}{K}\right]^2 - \frac{4}{K^2}A(t)B(t)}$$

$$= \sqrt{1 + 2\left[\frac{A(t)+B(t)}{K}\right] + \left[\frac{A(t)-B(t)}{K}\right]^2}. \tag{3}$$

As mentioned earlier, the tQSSA is generally more accurate than the conventional MM rate law [12,13,18–24]. To obtain the MM rate law, consider a rather specific condition,

$$B(t) \ll K + A(t) \text{ or } A(t) \ll K + B(t). \tag{4}$$

In this condition, the Padé approximant for $C_{tQ}(t)$ takes the following form:

$$C_{tQ}(t) \approx \frac{A(t)B(t)}{K+A(t)+B(t)}. \tag{5}$$

Considering Eq. (5), Eq. (4) is similar to the condition $C_{tQ}(t)/A(t) \ll 1$ or $C_{tQ}(t)/B(t) \ll 1$. In other words, Eq. (5) would be valid when the concentration of AB complex is negligible compared to either A or B's concentration. This condition is essentially identical to the assumption in the sQSSA resulting in the MM rate law [14]. In the example of a typical metabolic reaction with $B(t) \ll A(t)$ for substrate A and enzyme B, Eq. (4) is automatically satisfied and Eq. (5) further reduces to the familiar MM rate law $C_{tQ}(t) \approx A(t)B(t)/[K + A(t)]$, i.e., the outcome of the sQSSA [1–4,12–14]. To be precise, the sQSSA uses the concentration of free A instead of $A(t)$, but we refer to this formula with $A(t)$ as the sQSSA because the complex is assumed to be negligible in that scheme. Clearly, K here is the Michaelis constant, commonly known as K_M.

The application of the MM rate law beyond the condition in Eq. (4) invites a risk of erroneous modeling results, whereas the tQSSA is relatively free of such errors and has wider applicability [12,13,18–24]. Still, both the tQSSA and sQSSA stand on the quasi-steady state assumption that $C(t)$ approaches an equilibrium fast enough each time before the marked temporal change of $A(t)$ or $B(t)$. We now relax this assumption and generalize the

approximation of $C(t)$ to the case of time-varying $A(t)$ and $B(t)$, as the main objective of this study.

Suppose that $C(t)$ may not necessarily approach the equilibrium each time but stays within some distance from it. Revisiting Eq. (1), we derive the following approximant for $C(t)$ as explained in Supplementary Material, Section S1:

$$C_\gamma(t) \equiv \min\left\{C_{\mathrm{tQ}}\left\{t - \left[k_\delta \Delta_{\mathrm{tQ}}(t)\right]^{-1}\right\}, A(t), B(t)\right\}. \quad (6)$$

Although the above $C_\gamma(t)$ looks rather complex, this form is essentially a simple conversion $t \to t - \left[k_\delta \Delta_{\mathrm{tQ}}(t)\right]^{-1}$ in the tQSSA. $\min\{\cdot\}$ is just taken for a minor role to ensure that the complex concentration cannot exceed $A(t)$ or $B(t)$. Hence, the distinct feature of $C_\gamma(t)$ is the inclusion of an effective time delay $\left[k_\delta \Delta_{\mathrm{tQ}}(t)\right]^{-1}$ in complex formation. This delay is the rigorous estimate of the molecular relaxation time during which the effect of instantaneous $A(t)$ and $B(t)$ is notably sustained in the complex formation, as shown in Supplementary Material, Section S1. We will refer to this formulation as the effective time-delay scheme (ETS), and its relationship with the tQSSA is depicted in Fig. 1(A).

We propose the ETS as the generalization of the MM rate law for time-varying molecular concentrations that may not strictly adhere to the quasi-steady state assumption. If the relaxation time in complex formation is so short that the effective time delay in Eq. (6) can be ignored, the ETS returns to the tQSSA in its form. Surprisingly, we proved that, unlike the ETS, any simpler new rate law without a time-delay term would not properly work for active concentration changes over time (Supplementary Material, Section S3). Nevertheless, one may question the analytical utility of the ETS, regarding the apparent complexity of its time-delay term. In the examples of autogenously-regulated cellular adaptation and rhythmic protein turnover below, we will use the ETS to deliver valuable analytical insights into the systems whose dynamics is otherwise ill-explained by the conventional approaches.

About the physical interpretation of the ETS, we notice that the effective time delay is inversely linked to free molecule availability, as $\left[k_\delta \Delta_{\mathrm{tQ}}(t)\right]^{-1} = k_\delta^{-1}\left\{1 + K^{-1}\left[A(t) + B(t) - 2C_{\mathrm{tQ}}(t)\right]\right\}^{-1}$ from Eq. (2). Here, $A(t) + B(t) - 2C_{\mathrm{tQ}}(t) = \left[A(t) - C_{\mathrm{tQ}}(t)\right] + \left[B(t) - C_{\mathrm{tQ}}(t)\right]$, which approximates the total free molecule concentration near the equilibrium each time. In other words, the less the free molecules, the more the time delay, which is at most k_δ^{-1}. One can understand this observation as follows: given $A(t)$ and $B(t)$ at each moment, Eq. (1) indicates that the decay time-scale of the complex (k_δ^{-1}) is a main contributor to the relaxation time, which becomes further shortened as the complex formation itself decelerates with free molecule depletion over time. This depletion effect is

pronounced if the free molecule concentration is high (Supplementary Material, Section S1). Therefore, the relaxation time takes a decreasing function of the free molecule concentration, consistent with the above observation. Clearly, the free molecule concentration would be low for relatively few A and B molecules with comparable concentrations—i.e., small $A(t) + B(t)$ and $[A(t) - B(t)]^2$ in Eq. (3). In this case, the relaxation time would be relatively long and the ETS shall be deployed instead of the tQSSA or sQSSA. We thus expect that protein–protein interactions would often be the cases in need of the ETS compared to metabolic reactions with much excess substrates not binding to enzymes, as will be shown later.

Thus far, we have implicitly assumed the continuous nature of molecular concentrations as in Eq. (1). However, there exist biomolecular events that fundamentally deviate from this assumption. For example, a transcription factor (TF) binds to a DNA molecule in the nucleus to regulate mRNA expression and the number of such a TF–DNA assembly would be either 1 or 0 for a DNA site that can afford at most one copy of the TF [Fig. 1(B)]. This inherently discrete nature of the TF–DNA assembly is seemingly contrasted with the continuity of the molecular complex level in Eq. (1). To rigorously describe this TF–DNA binding dynamics, we harness the chemical master equation [29] and introduce quantities $A_{\mathrm{TF}}(t)$ and $C_{\mathrm{TF}}(t)$, which are the total TF concentration and the TF–DNA assembly concentration averaged over the cell population, respectively (Supplementary Material, Section S4). According to our calculation, the quasi-steady state assumption leads to the following approximant for $C_{\mathrm{TF}}(t)$:

$$C_{\mathrm{TFQ}}(t) \equiv \frac{A_{\mathrm{TF}}(t)}{V[K+A_{\mathrm{TF}}(t)]}, \tag{7}$$

where $K \equiv k_\delta/k_\mathrm{a}$ with k_a and k_δ as the TF–DNA binding and unbinding rates, respectively, and V is the nuclear volume (Supplementary Material, Section S4).

$C_{\mathrm{TFQ}}(t)$ in Eq. (7) looks very similar to the MM rate law, considering the "concentration" of the DNA site (V^{-1}). Nevertheless, $C_{\mathrm{TFQ}}(t)$ is not a mere continuum of Eq. (5), because the denominator in $C_{\mathrm{TFQ}}(t)$ includes $K + A_{\mathrm{TF}}(t)$, but not $K + A_{\mathrm{TF}}(t) + V^{-1}$. In fact, the discrepancy between $C_{\mathrm{TFQ}}(t)$ and Eq. (5) comes from the inherent stochasticity in the TF–DNA assembly (Supplementary Material, Section S4). In this regard, directly relevant to $C_{\mathrm{TFQ}}(t)$ is the stochastic version of the MM rate law with denominator $K + A(t) + B(t) - V^{-1}$ proposed by Levine and Hwa [30], because the DNA concentration $B(t)$ is V^{-1} in our case. $C_{\mathrm{TFQ}}(t)$ is a fundamentally more correct approximant for the DNA-binding TF level

than both the tQSSA and sQSSA in Eqs. (2) and (5). Therefore, we will just refer to $C_{\mathrm{TFQ}}(t)$ as the QSSA for TF–DNA interactions.

Still, the use of $C_{\mathrm{TFQ}}(t)$ stands on the quasi-steady state assumption. We relax this assumption and generalize the approximation of $C_{\mathrm{TF}}(t)$ to the case of time-varying TF concentration. As a result, we propose the following approximant for $C_{\mathrm{TF}}(t)$ (Supplementary Material, Section S4):

$$C_{\mathrm{TF}\gamma}(t) \equiv C_{\mathrm{TFQ}}\left[t - \frac{k_\delta^{-1}K}{K+A_{\mathrm{TF}}(t)}\right]. \tag{8}$$

This formula represents the TF–DNA version of the ETS, and its relationship with the QSSA is illustrated in Fig. 1(B). The time-delay term in Eq. (8) has a similar physical interpretation to that in Eq. (6). Besides, this term is directly proportional to the probability of the DNA unoccupancy in equilibrium, according to Eq. (7).

Through numerical simulations of various theoretical and empirical systems, we found that the ETS provides the reasonably accurate description of the deviations of time-course molecular profiles from the quasi-steady states (Supplementary Material, Sections S6–S8). This result was particularly evident for the cases of protein–protein and TF–DNA interactions with time-varying protein concentrations. In these cases, the ETS unveils the importance of the relaxation time (effective time delay) in complex formation to the shaping of molecular profiles, otherwise difficult to clarify. Yet, the use of the sQSSA or tQSSA is practically enough for typical metabolic reaction and transport systems, without the need for the ETS. The strict mathematical conditions for the validity of the ETS as well as those of the quasi-steady state assumption are derived in Supplementary Material, Section S5.

Autogenous control

Adaptation to changing environments is a process of biological control. The ETS offers an analytical tool for understanding transient dynamics of such adaptation processes, exemplified by autogenously regulated systems where TFs regulate their own transcription. This autogenous control underlies cellular responses to various internal and external stimuli [31,32]. We here explore the case of positive autoregulation and show that the quasi-steady state assumption does not even work for extremely-slow protein changes near a tipping point. The case of negative autoregulation is covered in Supplementary Material, Section S10.

In the case of positive autoregulation, consider a scenario in Fig. 2(A) that proteins enhance their own transcription after homodimer formation and this dimer–promoter interaction is

facilitated by inducer molecules. The inherent cooperativity from the dimerization is known to give a sigmoid TF–DNA binding curve, resulting in abrupt and history-dependent transition events [31,33]. We here built the full kinetic model of the system without the ETS, tQSSA, or other approximations of the dimerization and dimer–promoter interaction (Supplementary Material, Section S9). As the simulated inducer level increases, Fig. 2(B) demonstrates that an initially low, steady-state protein level undergoes an abrupt leap at some point η_c, known as a transition or tipping point. This discontinuous transition with only a slight inducer increase signifies a qualitative change in the protein expression state. Reducing the inducer level just back to the transition point η_c does not reverse the protein state, which is sustained until more reduction in the inducer level [Fig. 2(B)]. This history-dependent behavior, hysteresis, indicates the coexistence of two different stable states of the protein level (bistability) between the forward and backward transitions [31,33].

Other than steady states, we examine how fast the system responds to signals. Upon acute induction from a zero to certain inducer level ($> \eta_c$), the protein level grows over time towards its new steady state and this response becomes rapider at stronger induction away from the transition point [Fig. 2(C)]. Conversely, as the inducer level decreases towards the transition point, the response time continues to increase and eventually becomes diverging (in this study, response time is defined as the time taken for a protein level to reach 90% of its steady state). This phenomenon has been called “critical slowing down” [34–36]. Regarding this near-transition much slow protein growth, one may expect that the quasi-steady state assumption would work properly near that transition point. To test this possibility, we modified the full model by the tQSSA and QSSA of the dimerization and dimer-promoter interaction, respectively, and call this modified model the QSSA-based model. For comparison, we created another version of the model by the ETS of the dimerization and dimer-promoter interaction and call this version the ETS-based model (Supplementary Material, Section S9). Across physiologically-relevant parameter conditions, we compared the QSSA- and ETS-based model simulation results to the full model’s (Supplementary Material, Section S12 and Table S5). Surprisingly, the QSSA-based model often severely underestimated the response time, particularly near a transition point, while the ETS-based response time was relatively close to that from the full model [$P < 10^{-4}$ and Supplementary Material, Section S12; e.g., 8.5-hour shorter and 0.5-hour longer response times in Fig. 2(C) (left) in the QSSA and ETS cases, respectively].

This unexpected mismatch between the QSSA and full model results comes from the following factors: because the QSSA model discards the effective time delay in dimerization and dimer-promoter interaction, this model accelerates positive feedback, transcription, and

protein production, and thus shortens the response time. Near the transition point, although the protein level grows very slowly, a little higher transcription activity in the QSSA model substantially advances the protein growth with near-transition ultrasensitivity that we indicated above. Therefore, the QSSA model shortens the response time even near the transition point.

Related to this point, the ETS allows the analytical calculation of response time and its QSSA-based estimate. In this calculation, we considered two different stages of protein growth—its early and late stages [Fig. 2(D)] and found that the QSSA model underestimates response time mainly at the early stage. This calculation suggests that the exact response time would be longer than the QSSA-based estimate by

$$\frac{2\pi}{r\sqrt{\frac{\eta-\eta_c}{\eta_c}}}\left(\frac{1}{D}+\frac{1}{D_{TF}}\right)+\frac{1}{r}\ln\left(1+\frac{1}{D}+\frac{1}{D_{TF}}\right)+\frac{1}{r}\left(\frac{1}{D}+\frac{1}{D_{TF}}\right)\ln\left\{1+\frac{DD_{TF}(\bar{u}-1)[DD_{TF}(\bar{u}-1)-2(D+D_{TF})]}{(D+D_{TF})^2}\right\}, \quad (9)$$

where η and η_c denote an inducer level and its value at the transition point, respectively, r is the sum of protein degradation and dilution rates, and D and D_{TF} are parameters inversely proportional to the effective time delays in dimerization and dimer–promoter interaction, respectively. The additional details and the definition of parameter $\bar{u}$ are provided in Supplementary Material, Section S9.

Notably, the above response time difference vanishes as $D^{-1}+D_{TF}^{-1}\to 0$. In other words, the total effective time delay is responsible for this response time difference. Strikingly, this difference indefinitely grows as η decreases towards η_c, as a linear function of $1/\sqrt{(\eta-\eta_c)/\eta_c}$. This prediction can serve as a testbed for our theory and highlights far excessive elongation of near-transition response time (compared to the QSSA) as an amplified effect of the relaxation time in complex formation. This amplified effect is the result of the near-transition ultrasensitivity that we indicated above. Consistent with our prediction, the full model simulation always shows longer response time than the QSSA model simulation and the difference is linearly scaled to $1/\sqrt{(\eta-\eta_c)/\eta_c}$ as exemplified by Fig. 2(E) ($R^2>0.98$ in simulated conditions; see Supplementary Material, Section S12). Moreover, its predicted slope against $1/\sqrt{(\eta-\eta_c)/\eta_c}$ [i.e., 2π ($6.28\cdots$) multiplied by $\left(D_{TF}^{-1}+D^{-1}\right)r^{-1}$] is comparable with the simulation results [7.3 ± 0.3 (avg. ± s.d. in simulated conditions) multiplied by $\left(D_{TF}^{-1}+D^{-1}\right)r^{-1}$; see Supplementary Material, Section S12]. The agreement of these nontrivial predictions with the numerical simulation results proves the theoretical value of the ETS. Again, we raise a caution against the quasi-steady state assumption, which unexpectedly fails for very slow dynamics with severe underestimation of response time, e.g., by a few tens of hours in the case of Fig. 2(E).

Rhythmic degradation of circadian proteins

Circadian clocks in various organisms generate endogenous molecular oscillations with ~24 h periodicity, enabling physiological adaptation to diurnal environmental changes caused by the Earth's rotation around its axis. Circadian clocks play a pivotal role in maintaining biological homeostasis, and the disruption of their function is associated with a wide range of pathophysiological conditions [7,9,18,25–27]. According to previous reports, some circadian clock proteins are not only rhythmically produced but also decompose with rhythmic degradation rates [Figs. 3(A) and 3(B)] [37–41]. Recently, we have suggested that the rhythmic degradation rates of proteins with circadian production can spontaneously emerge without any explicitly time-dependent regulatory mechanism of the degradation processes [37,42]. If the rhythmic degradation rate peaks at the descending phase of the protein profile and stays relatively low elsewhere, it is supposed to save much of the biosynthetic cost in maintaining a circadian rhythm. A degradation mechanism with multiple post-translational modifications (PTMs), such as phospho-dependent ubiquitination, may elevate the rhythmicity of this degradation rate in favor of the biosynthetic cost saving [37,40]. Can the ETS explain this inherent rhythmicity in the degradation rates of circadian proteins?

First, we constructed the kinetic model of circadian protein production and degradation without the ETS or other approximations (Supplementary Material, Section S11). This model attributes a circadian production rate of the protein to a circadian mRNA expression or translation rate. Yet, a protein degradation rate in the model is not based on any explicitly time-dependent regulatory processes, but on constantly-maintained proteolytic mediators such as constant E3 ubiquitin ligases and kinases. In realistic situations, the protein turnover may require multiple preceding PTMs, like mono- or multisite phosphorylation and subsequent ubiquitination. Our model covers these cases, as well.

Next, we apply the ETS to the PTM processes in the model for the analytical estimation of the protein degradation rate. We observed the mathematical equivalence of the PTM processes and the above-discussed TF–DNA interactions, despite their different biological contexts (Supplementary Material, Section S11). This observation leads to the estimate $r_\gamma(t)$ of the protein degradation rate as

$$r_\gamma(t) \equiv \frac{a_v}{A(t)} \min\left[\frac{a_u}{a_u+a_v} A\left(t-\frac{1}{a_u+a_v}\right), A(t)\right] \approx \frac{a_u a_v}{a_u+a_v}\left\{1-\frac{1}{a_u+a_v}\left[\frac{1}{A(t)}\frac{\mathrm{d}A(t)}{\mathrm{d}t}\right]+\cdots\right\}, \quad (10)$$

where $A(t)$ is a protein concentration, a_u and a_v are the rates of the two slowest PTM and turnover steps in a protein degradation pathway (the step of a_u precedes that of a_v in the

degradation pathway; see Supplementary Material, Section S11), and the rightmost formula is to simplify $r_\gamma(t)$ with the Taylor expansion. The use of $r_\gamma(t)$ may not satisfactorily work for the degradation depending on many preceding PTMs, but still helps to capture the core feature of the dynamics.

Strikingly, the quasi-steady state assumption does not predict a rhythmic degradation rate, as the QSSA version of Eq. (10) gives rise to a constant degradation rate, $a_u a_v/(a_u + a_v)$ (Supplementary Material, Section S11). In contrast, the ETS naturally accounts for the degradation rhythmicity through the effective time delay in the degradation pathway. The rightmost formula in Eq. (10) indicates that the degradation rate would be an approximately increasing function of $-A'(t)/A(t)$ and thus increase as time goes from the ascending to descending phase of the protein profile. This predicted tendency well matches the experimental data patterns in Figs. 3(A) and 3(B). Fundamentally, this degradation rhythmicity roots in the unsynchronized interplay between protein translation, modification, and turnover events [37]. For example, in the case of protein ubiquitination, ubiquitin ligases with a finite binding affinity would not always capture all newly-translated substrates, and therefore a lower proportion of the substrates can be ubiquitinated during the ascending phase of the substrate profile than during the descending phase. The degradation rate partially follows this ubiquitination pattern. Additional PTMs like phosphorylation, if required for the ubiquitination, can further retard the full substrate modification and thereby increase the degradation rhythmicity for a given substrate profile. One may expect that these effects would be enhanced with more limited ubiquitin ligases or kinases, under the condition when the substrate level shows a strong oscillation. This expectation is supported by the relative amplitude of the degradation rate estimated by Eq. (10):

$$\frac{\max_t[r_\gamma(t)]-\min_t[r_\gamma(t)]}{\langle r_\gamma(t)\rangle} \approx \frac{1}{a_u+a_v}\left\{\max_t\left[\frac{1}{A(t)}\frac{\mathrm{d}A(t)}{\mathrm{d}t}\right]-\min_t\left[\frac{1}{A(t)}\frac{\mathrm{d}A(t)}{\mathrm{d}t}\right]\right\}, \tag{11}$$

where $\langle\cdot\rangle$ denotes a time average. Here, the relative amplitude of the degradation rate is proportional to $1/(a_u + a_v)$ as well as to the amplitude of $A'(t)/A(t)$. Therefore, limited ubiquitin ligases or kinases, and strong substrate oscillations increase the rhythmicity of the degradation rate. Given a substrate profile, multiple PTMs can further enhance this degradation rhythmicity because they invite the possibility of smaller a_u and a_v values than expected for the case of only a single PTM. Moreover, Eq. (10) predicts that the degradation rate would peak around the peak time of $-A'(t)/A(t)$.

In the example of Fig. 3(C) for a single PTM case, the simulated degradation rate from the aforementioned full kinetic model exhibits the rhythmic profile in excellent agreement with

the ETS-predicted profile. Notably, the peak time of the simulated degradation rate is very close to that of $-A'(t)/A(t)$ as predicted by the ETS. Indeed, the peaks of the degradation rates show only < 1h time differences from the maximum $-A'(t)/A(t)$ values across most (89–99%) of the simulated conditions of single to triple PTM cases [Fig. 3(D); Supplementary Material, Section S12 and Table S6]. In addition, for each substrate profile, the simulated degradation rate tends to become more rhythmic and have a larger relative amplitude as the number of the PTMs increases [Fig. 3(E)], supporting the above argument that multiple PTMs can facilitate degradation rhythmicity. The estimated relative amplitude in Eq. (11) also shows this tendency for single to double PTMs, yet not clearly for triple PTMs unlike the simulated relative amplitude [Fig. 3(E)]. This inaccuracy with the triple PTMs comes from the accumulated errors over multiple PTMs in our estimation, as we indicated early. Still, the estimate in Eq. (11) accounts for at least the order of magnitude of the simulated relative amplitude, as the ratio of the simulated to estimated relative amplitude almost equals 1 for a single PTM case and remains to be $O(1)$ for double and triple PTM cases [Fig. 3(F)].

Together, the ETS provides a useful theoretical framework of rhythmic degradation of circadian proteins, which is hardly explained by the quasi-steady state assumption.

Parameter estimation

The use of an accurate function of variables and parameters is important for good parameter estimation by the fitting of the parameters [13,43,44]. Parameter estimation is a crucial part of pharmacokinetic–pharmacodynamic (PK–PD) analysis for drug development and clinical study design. Yet, the MM rate law is widely deployed for PK–PD models integrated into popular simulation and statistical analysis tools.

To raise a caution against the unconditional use of the quasi-steady state assumption in parameter estimation, we here compare the accuracies of the tQSSA- and ETS-based parameter estimates. Because the sQSSA-based parameter estimates have already been known as less accurate than the tQSSA-based ones [12,44], we skip the use of the sQSSA. Specifically, we consider a protein–protein interaction model with time-varying protein concentrations (Supplementary Material, Section S12). To the "true" profile of the protein complex [i.e., $C(t)$ in Eq. (1)], we fit the ETS [$C_\gamma(t)$ in Eq. (6)] or the tQSSA [$C_{\mathrm{tQ}}(t)$ in Eq. (2)] and estimate the original parameters of the model [45]: the ETS-based fitting can estimate both parameters K and k_δ, and the tQSSA-based fitting can estimate only K.

Likewise, we consider a TF–DNA interaction model with time-varying TF concentration (Supplementary Material, Section S12). The ETS-based fitting can estimate both K and k_δ, and the QSSA-based fitting can estimate only K.

In the case of protein–protein interactions, Fig. 4(A) reveals that the ETS improves the parameter estimation over the tQSSA, with the tendency of more accurate estimation of K. For example, in the cases that the relative error of K estimated by the tQSSA is ≥ 0.2, most of the ETS-based estimates (75.9%) show the relative error < 0.2 ($P < 10^{-4}$ and Supplementary Material, Section S12) and their 65.9% even show the relative error < 0.1. In the case of TF–DNA interactions, the ETS still offers an improvement in the estimation of K, but this improvement is comparably weak [Fig. 4(B)].

Unlike K, k_δ can only be estimated through the ETS, and hence the comparison to the tQSSA- or QSSA-based estimate is not possible. Still, k_δ is found to have the relative error < 0.1 for most of the ETS-based estimates, 86.6% and 80.7% in the cases of protein–protein and TF–DNA interactions, respectively [Figs. 4(C) and 4(D)].

Discussion

The quasi-steady state assumption involves the approximation by time-scale separation where the "fast" components of a system undergo instantaneous equilibrium and only the "slow" components govern the relevant dynamics. The time-scale separation has been a long practice in many different areas, such as the Monod–Wyman–Changeux model of allosteric effects, the Ackers–Johnson–Shea model of gene regulation by λ phage repressor, and the Born–Oppenheimer approximation in quantum chemistry [46–48]. If some prediction from the time-scale separation deviates from empirical data, our study may provide a useful intuition about this deviation based on an overlooked time-delay effect in that system.

We here proposed the ETS as a theoretical framework of molecular interaction kinetics with time-varying molecular concentrations. The utility of the ETS for transient or oscillatory dynamics originates in the rigorous estimation of the relaxation time in complex formation, i.e., the effective time delay. In the cases of protein–protein and TF–DNA interactions, the ETS manifests the importance of the effective time delay for the time-course molecular profiles distinct from the quasi-steady states. Accordingly, the ETS provides valuable analytical insights into the signal response time under autogenous regulation and the spontaneous establishment of the rhythmic degradation rates of circadian proteins. In addition, the ETS improves kinetic parameter estimation with a caution against the unconditional use of the quasi-steady state assumption. Our approach enhances the mathematical understanding of the time-varying behaviors of complex-complete mass-action models [33,37,49] beyond only their steady states.

Further elaboration and physical interpretation of our framework, in concert with extensive experimental profiling of molecular complexes in regulatory or signaling pathways

[15,16], are warranted for the correct explanation of the interplay of cellular components and its functional consequences. Although the simulation and empirical data presented here are supportive of the ETS, experimental tests including direct validation are clearly warranted. This validation could involve the measurements of the time-series of molecular complex concentrations by co-immunoprecipitation assays or other techniques. High temporal resolution data are preferred for their comparison with the ETS-based profiles. Lastly, comprehensive consideration of stochastic fluctuation and nonlinearity in molecular binding events [29,50,51] would be a fruitful endeavor for more complete development of our theory, although the stochasticity in TF–DNA interactions was partially considered in this work.

Materials and methods

The full details of theory derivation, mathematical modeling, and data sources are available in Supplementary Material. Numerical simulation and data analysis methods are presented in Supplementary Material, Section S12: briefly, simulations and data analyses were performed by Python 3.7.0 or 3.7.4. Ordinary differential equations were solved by LSODA (scipy.integrate.solve_ivp) in SciPy v1.1.0 or v1.3.1 with the maximum time step of 0.05 h. Delay differential equations were solved by a modified version of the ddeint module with LSODA [52]. Splines of discrete data points were achieved with scipy.interpolate.splrep in SciPy v1.3.1. Linear regression of data points was performed with scipy.stats.linregress in SciPy v1.3.1 and then the slope of the fitted line and R^2 were obtained. For the parameter selection in numerical simulations or for the null model generation in statistical significance tests, random numbers were sampled by the Mersenne Twister in random.py. To test the significance of the average of the relative errors of analytical estimates against actual simulation data, we randomized the pairing of these estimates and simulation data (while maintaining their identities as the estimates and simulation data) and measured the P value (one-tailed) from the 10^4 null configurations.

The source codes will be uploaded to GitHub before the manuscript publication.

Acknowledgements

We thank Haneul Kim for useful discussions. This work was supported by Hong Kong Baptist University, Startup Grant Tier 2 (RC-SGT2/18-19/SCI/001) (R.L., T.L.P.M., and P.-J.K.), the Health and Medical Research Fund (HMRF 17182691) (R.L. and P.-J.K.), and the National Research Foundation of Korea Grants (NRF-2020R1A4A1019140, NRF-2020R1F1A1075942, and NRF-2018K1A4A3A01063890) funded by the Ministry of Science and ICT (J.C., W.J.K.,

and C.-M.G). This work was partially conducted with the resources of the High Performance Cluster Computing Centre, Hong Kong Baptist University, which receives funding from Research Grant Council, University Grant Committee of the HKSAR and Hong Kong Baptist University. We also acknowledge the support of the UNIST Supercomputing Center for the computing resources.

References

1. V. Henri, *Lois Générales de l'Action des Diastases* (Librairie Scientifique A. Hermann, 1903).
2. L. Michaelis and M. L. Menten, *Die Kinetik der Invertinwirkung*, Biochem. Z. **49**, 333–369 (1913).
3. G. E. Briggs and J. B. S. Haldane, *A Note on the Kinetics of Enzyme Action*, Biochem. J. **19**, 338 (1925).
4. J. Gunawardena, *Time-Scale Separation–Michaelis and Menten's Old Idea, Still Bearing Fruit*, FEBS. J. **281**, 473–488 (2014).
5. C. Gérard and A. Goldbeter, *A Skeleton Model for the Network of Cyclin-Dependent Kinases Driving the Mammalian Cell Cycle*, Interface Focus **1**, 24–35 (2011).
6. K. C. Chen, A. Csikasz-Nagy, B. Gyorffy, J. Val, B. Novak, and J. J. Tyson, *Kinetic Analysis of a Molecular Model of the Budding Yeast Cell Cycle*, Mol. Biol. Cell **11**, 369–391 (2000).
7. J. C. Leloup and A. Goldbeter, *Toward a Detailed Computational Model for the Mammalian Circadian Clock*, Proc. Natl. Acad. Sci. USA **100**, 7051–7056 (2003).
8. J. Garcia-Ojalvo, *Modeling Gene Expression in Time and Space*, Annu. Rev. Biophys. **42**, 605–627 (2013).
9. M. Foo, D. E. Somers, and P.-J. Kim, *Kernel Architecture of the Genetic Circuitry of the Arabidopsis Circadian System*, PLoS Comput. Biol. **12**, e1004748 (2016).
10. T. D. Pollard, *A Guide to Simple and Informative Binding Assays*, Mol. Biol. Cell **21**, 4061–4067 (2010).
11. A. D. Attie and R. T. Raines, *Analysis of Receptor–Ligand Interactions*, J. Chem. Educ. **72**, 119 (1995).
12. J. K. Kim and J. J. Tyson, *Misuse of the Michaelis–Menten Rate Law for Protein Interaction Networks and Its Remedy*, PLoS Comput. Biol. **16**, e1008258 (2020).
13. S. Schnell and P. K. Maini, *A Century of Enzyme Kinetics: Reliability of the K_M and v_{max} Estimates*, Comm. Theor. Biol. **8**, 169–187 (2003).

14. L. A. Segel and M. Slemrod, *The Quasi-Steady-State Assumption: a Case Study in Perturbation*, SIAM Rev. **31**, 446–477 (1989).
15. A. Fujioka, K. Terai, R. E. Itoh, K. Aoki, T. Nakamura, S. Kuroda *et al.*, *Dynamics of the Ras/ERK MAPK Cascade as Monitored by Fluorescent Probes*, J. Biol. Chem. **281**, 8917–8926 (2006).
16. N. Blüthgen, F. J. Bruggeman, S. Legewie, H. Herzel, H. V. Westerhoff, and B. N. Kholodenko, *Effects of Sequestration on Signal Transduction Cascades*, FEBS J. **273**, 895–906 (2006).
17. S. Carmi, E. Y. Levanon, S. Havlin, and E. Eisenberg, *Connectivity and Expression in Protein Networks: Proteins in a Complex Are Uniformly Expressed*, Phys. Rev. E. **73**, 031909 (2006).
18. J. K. Kim and D. B. Forger, *A Mechanism for Robust Circadian Timekeeping via Stoichiometric Balance*, Mol. Syst. Biol. **8**, 630 (2012).
19. J. A. M. Borghans, R. J. de Boer, and L. A. Segel, *Extending the Quasi-Steady State Approximation by Changing Variables*, Bull. Math. Biol. **58**, 43–63 (1996).
20. N. E. Buchler and M. Louis, *Molecular Titration and Ultrasensitivity in Regulatory Networks*, J. Mol. Biol. **384**, 1106–1119 (2008).
21. A. R. Tzafriri, *Michaelis–Menten Kinetics at High Enzyme Concentrations*, Bull. Math. Biol. **65**, 1111–1129 (2003).
22. H. C. Lim, *On Kinetic Behavior at High Enzyme Concentrations*, AICHE J. **19**, 659–661 (1973).
23. S. Cha, *Kinetic Behavior at High Enzyme Concentrations: Magnitude of Errors of Michaelis–Menten and Other Approximations*, J. Biol. Chem. **245**, 4814–4818 (1970).
24. K. J. Laidler, *Theory of the Transient Phase in Kinetics, with Special Reference to Enzyme Systems*, Can. J. Chem. **33**, 1614–1624 (1955).
25. F. Gachon, E. Nagoshi, S. Brown, J. Ripperger, and U. Schibler, *The Mammalian Circadian Timing System: From Gene Expression to Physiology*, Chromosoma **113**, 103–112 (2004).
26. D. H. Nagel and S. A. Kay, *Complexity in the Wiring and Regulation of Plant Circadian Networks*, Curr. Biol. **22**, R648–R657 (2012).
27. T. S. Hatakeyama and K. Kaneko, *Reciprocity between Robustness of Period and Plasticity of Phase in Biological Clocks*, Phys. Rev. Lett. **115**, 218101 (2015).
28. N. Mosheiff, B. M. C. Martins, S. Pearl-Mizrahi, A. Grünberger, S. Helfrich, I. Mihalcescu, D. Kohlheyer, J. C. W. Locke, L. Glass, and N. Q. Balaban, *Inheritance of Cell-Cycle Duration in the Presence of Periodic Forcing*, Phys. Rev. X **8**, 021035 (2018).

29. V. Kampen and N. Godfried, *Stochastic Processes in Physics and Chemistry* (Elsevier, 1992).
30. E. Levine and T. Hwa, *Stochastic Fluctuations in Metabolic Pathways*, Proc. Natl. Acad. Sci. USA **104**, 9224–9229 (2007).
31. Y. T. Maeda and M. Sano, *Regulatory Dynamics of Synthetic Gene Networks with Positive Feedback*, J. Mol. Biol. **359**, 1107–1124 (2006).
32. N. Rosenfeld, M. B. Elowitz, and U. Alon, *Negative Autoregulation Speeds the Response Times of Transcription Networks*, J. Mol. Biol. **323**, 785–793 (2002).
33. C. Jeynes-Smith and R. P. Araujo, *Ultrasensitivity and Bistability in Covalent-Modification Cycles with Positive Autoregulation*, Proc. R. Soc. A **477**, 20210069 (2021).
34. F. Nazarimehr, S. Jafari, M. Perc, and J. C. Sprott, *Critical Slowing Down Indicators*, Europhys. Lett. **132**, 18001 (2020).
35. M. I. Maturana, C. Meisel, K. Dell, P. J. Karoly, W. D'Souza, D. B. Grayden, A. N. Burkitt, P. Jiruska, J. Kudlacek, J. Hlinka *et al.*, *Critical Slowing Down as a Biomarker for Seizure Susceptibility*, Nat. Commun. **11**, 1–12 (2020).
36. M. Scheffer, *Foreseeing Tipping Points*, Nature **467**, 411–412 (2010).
37. R. Lim, J. Chae, D. E. Somers, C.-M. Ghim, and P.-J. Kim, *Cost-Effective Circadian Mechanism: Rhythmic Degradation of Circadian Proteins Spontaneously Emerges without Rhythmic Post-Translational Regulation*, iScience **24**, 102726 (2021).
38. M. Zhou, J. K. Kim, G. W. Eng, D. B. Forger, and D. M. Virshup, *A Period2 Phosphoswitch Regulates and Temperature Compensates Circadian Period*, Mol. Cell **60**, 77–88 (2015).
39. E. M. Farre´ and S. A. Kay, *PRR7 Protein Levels Are Regulated by Light and the Circadian Clock in Arabidopsis*, Plant J. **52**, 548–560 (2007).
40. H.-H. Jo, Y. J. Kim, J. K. Kim, M. Foo, D. E. Somers, and P.-J. Kim, *Waveforms of Molecular Oscillations Reveal Circadian Timekeeping Mechanisms*, Commun. Biol. **1**, 207 (2018).
41. G. van Ooijen, L. E. Dixon, C. Troein, and A. J. Millar, *Proteasome Function Is Required for Biological Timing throughout the Twenty-Four Hour Cycle*, Curr. Biol. **21**, 869–875 (2011).
42. J. Chae, R. Lim, C.-M. Ghim, and P.-J. Kim, *Backward Simulation for Inferring Hidden Biomolecular Kinetic Profiles*, STAR Protoc. **2**, 100958 (2021).
43. W. Stroberg and S. Schnell, *On the Estimation Errors of K_M and V from Time-Course Experiments Using the Michaelis–Menten Equation*, Biophys. Chem. **219**, 17 (2016).
44. B. Choi, G. A. Rempala, and J. K. Kim, *Beyond the Michaelis–Menten Equation: Accurate and Efficient Estimation of Enzyme Kinetic Parameters*, Sci. Rep. **7**, 1–11 (2017).
45. M. J. D. Powell, *An Efficient Method for Finding the Minimum of a Function of Several Variables without Calculating Derivatives*, Comput. J. **7**, 155–162 (1964).

604 46. J. Monod, J. Wyman, and J.-P. Changeux, *On the Nature of Allosteric Transitions: A*
605 *Plausible Model*, J. Mol. Biol. **12**, 88–118 (1965).
606 47. G. K. Ackers, A. D. Johnson, and M. A. Shea, *Quantitative Model for Gene Regulation by λ*
607 *Phage Repressor*, Proc. Natl. Acad. Sci. USA **79**, 1129–1133 (1982).
608 48. M. Born and R. Oppenheimer, *Zur Quantentheorie der Molekeln*, Ann. Phys. **389**, 457–484
609 (1927).
610 49. A. K. Manrai and J. Gunawardena, *The Geometry of Multisite Phosphorylation*, Biophys. J.
611 **95**, 5533–5543 (2008).
612 50. C.-M. Ghim and E. Almaas, *Two-Component Genetic Switch as a Synthetic Module with*
613 *Tunable Stability*, Phys. Rev. Lett. **103**, 028101 (2009).
614 51. P.-J. Kim and N. D. Price, *Macroscopic Kinetic Effect of Cell-to-Cell Variation in*
615 *Biochemical Reactions*, Phys. Rev. Lett. **104**, 148103 (2010).
616 52. Scipy-based delay differential equation (dde) solver, https://github.com/Zulko/ddeint.
617 53. N. Nakamichi *et al*., *PSEUDO-RESPONSE REGULATORS 9, 7, and 5 Are Transcriptional*
618 *Repressors in the Arabidopsis Circadian Clock*, Plant Cell **22**, 594–605 (2010).

Figures

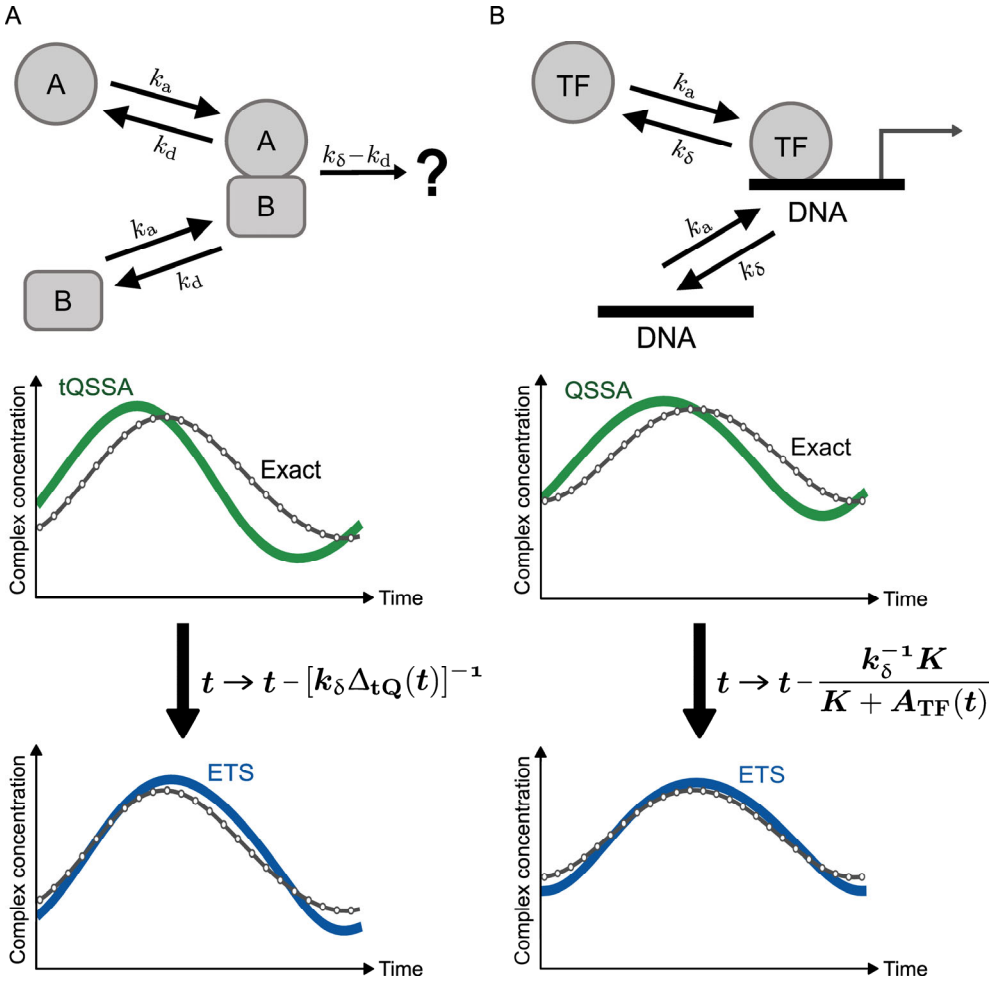

Fig. 1. Generalization of the MM rate law for time-varying molecular concentrations, referred to as the ETS. (A) Two different molecules A and B bind to each other and form their complex. (B) A TF binds to a DNA molecule to regulate mRNA expression (RNA polymerase and other molecules are omitted here). In (A) and (B), the graphs show the comparison among the exact time-course profile of the complex concentration, the tQSSA-based (A) or QSSA-based (B) profile, and the ETS-based profile. The relationship between the tQSSA (or QSSA) and the ETS is illustrated through the effective time delay in the ETS. Notations k_a, k_d, k_δ, t, $\Delta_{tQ}(t)$, K, and $A_{TF}(t)$ are defined in the description of Eqs. (1)–(3) and (6)–(8).

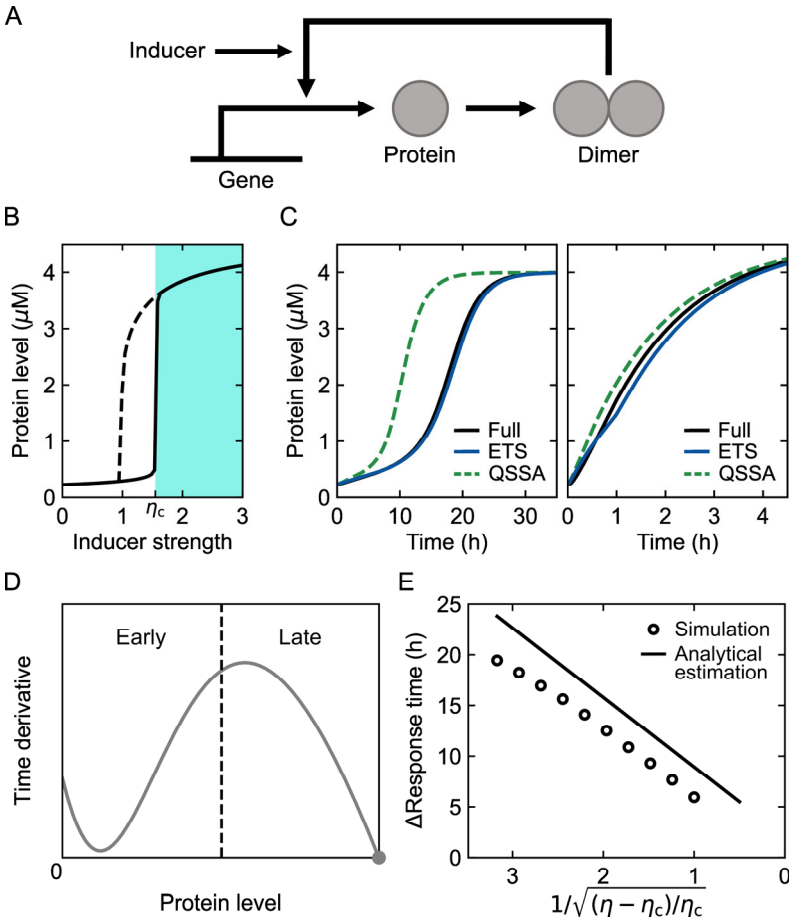

Fig. 2. Positive autoregulation and induction kinetics. (A) Protein production mechanism with positive autoregulation in the presence of inducers. (B) Bifurcation diagram of the simulated protein level as a function of η (proxy for an inducer level). The steady state is plotted as η increases (solid line) or decreases (dashed line). Acute induction can be simulated by a sudden change of $\eta = 0$ to $\eta > \eta_c$ in the shaded area. (C) Time-series of protein levels from the full, ETS, and QSSA models upon acute induction at time 0 h with $\eta = 2.42$ (left) or $\eta = 200$ (right). (D) Phase portrait of induction kinetics with $\eta > \eta_c$. A vertical dashed line splits the early and late stages of protein growth. A stable fixed point is indicated by a filled circle. (E) The full model-to-QSSA difference in response time as a function of $1/\sqrt{(\eta - \eta_c)/\eta_c}$. Both the simulated and analytically-estimated differences are presented. The analytical estimation is based on Eq. (9). For more details of (B)–(E), refer to Supplementary Material, Section S9 and Table S7.

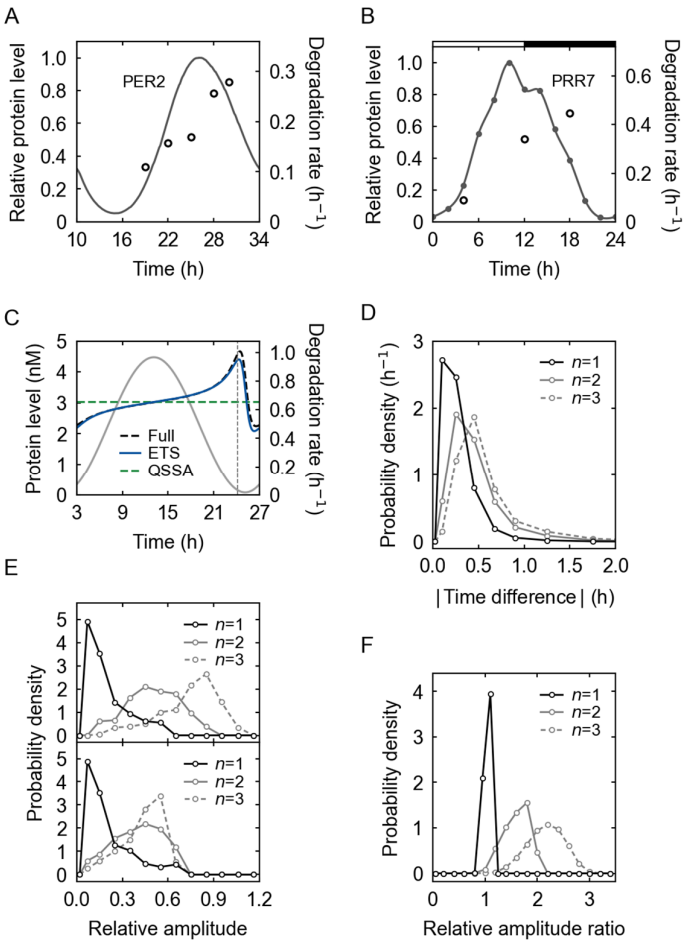

Fig. 3. Rhythmic degradation of circadian proteins. (A) The experimental abundance levels (solid line) and degradation rates (open circles) of the mouse PERIOD2 (PER2) protein [38]. (B) The experimental abundance levels (dots, interpolated by a solid line) and degradation rates (open circles) of PSEUDO RESPONSE REGULATOR 7 (PRR7) protein in *Arabidopsis thaliana* [39,40,53]. Horizontal white and black segments correspond to light and dark intervals, respectively. (C) A simulated protein degradation rate from the full kinetic model and its ETS- and QSSA-based estimates, when the degradation depends on a single PTM. In addition, the protein abundance profile is presented here (gray solid line). A vertical dashed line corresponds to the peak time of $-A'(t)/A(t)$ where $A(t)$ is a protein abundance. The parameters are provided in Supplementary Material, Table S8. (D) The probability distribution of the peak-time difference between a degradation rate and $-A'(t)/A(t)$ for each number of PTMs (n) required for the degradation. The probability distribution was obtained with randomly-sampled parameter sets in Supplementary Material, Table S6. (E) The probability distribution of the relative amplitude of a simulated degradation rate (top) or its estimate in Eq. (11) (bottom) for each n, when the relative amplitude of a protein abundance is 1. (F) The probability distribution of the ratio of the simulated to estimated

672 relative amplitude of a degradation rate for each n. For more details of (A)–(F), refer to
673 Supplementary Material, Section S11.
674
675
676

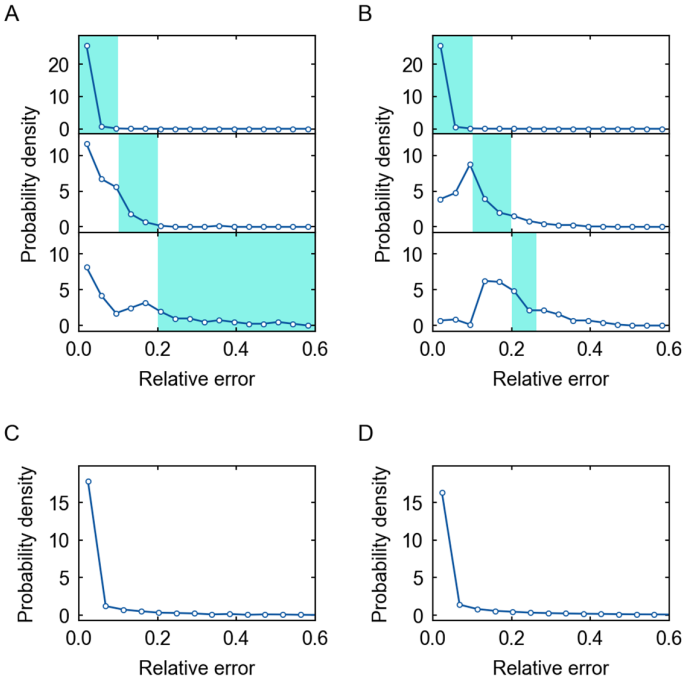

677
678
679 **Fig. 4.** Parameter estimation for protein–protein and TF–DNA interaction models. (A) The
680 probability distribution of the relative error of the ETS-estimated K for a protein–protein
681 interaction model. The estimation was conducted when the relative error of the tQSSA-
682 estimated K was < 0.1 (top), ≥ 0.1 and < 0.2 (center), or ≥ 0.2 (bottom). (B) The probability
683 distribution of the relative error of the ETS-estimated K for a TF–DNA interaction model. The
684 estimation was conducted when the relative error of the QSSA-estimated K was < 0.1 (top),
685 ≥ 0.1 and < 0.2 (center), or ≥ 0.2 (bottom). In (A) and (B), shaded is the literal range of the
686 relative error of the tQSSA-estimated (A) or QSSA-estimated (B) K from our simulated
687 conditions. More than a half of the simulated conditions show that the relative error of the
688 ETS-estimated K is < 0.1 (top and center) or < 0.2 (bottom). (C) The probability distribution of
689 the relative error of the ETS-estimated k_δ for the protein–protein interaction model in (A).
690 (D) The probability distribution of the relative error of the ETS-estimated k_δ for the TF–DNA
691 interaction model in (B). Although not shown in (C) and (D), there exist a negligible portion of
692 the simulated conditions where the relative error of the estimated k_δ is > 0.6. For more
693 details of (A)–(D), refer to Supplementary Material, Section S12.